Compact Mid-wave Imaging System (CMIS) for Retrieval of Cloud Motion Vectors and Cloud Geometric Heights

Michael A. Kelly[a], Dong Wu[b], Arnold Goldberg[a], Ivan Papusha[a], John Wilson[a], James Carr[d], John Boldt[a], Jacob Greenberg[a], Frank Morgan[a], Sam Yee[a], Andrew Heidinger[c], Lauren Mehr[a]

[a]Johns Hopkins University - Applied Physics Lab, Space Exploration Sector, 11100 Johns Hopkins Road, Laurel, MD 20723, USA

[b]NASA Goddard Space Flight Center, 8800 Greenbelt, Rd., Greenbelt, MD 20771, USA

[c]National Oceanographic and Atmospheric Administration, 1225 West Dayton St., Madison, WI, 53706, USA

[d]Carr Astronautics, 6404 Ivy Lane, #333, Greenbelt, MD, 20770, USA[d]

ABSTRACT

The Johns Hopkins University Applied Physics Laboratory (JHU/APL) is developing a compact, light-weight, and low-power midwave-infrared (MWIR) imager called the Compact Midwave Imaging Sensor (CMIS), under the support of the NASA Earth Science Technology Office Instrument Incubator Program. The goal of this CMIS instrument development and demonstration project is to increase the technical readiness of CMIS, a multi-spectral sensor capable of retrieving 3D winds and cloud heights 24/7, for a space mission. The CMIS instrument employs an advanced MWIR detector that requires less cooling than traditional technologies and thus permits a compact, low-power design, which enables accommodation on small spacecraft such as CubeSats. CMIS provides the critical midwave component of a multi-spectral sensor suite that includes a high-resolution Day-Night Band and a longwave infrared (LWIR) imager to provide global cloud characterization and theater weather imagery. In this presentation, an overview of the CMIS project, including the high-level sensor design, the concept of operations, and measurement capability will be presented. System performance for a variety of different scenes generated by a cloud resolving model (CRM) will also be discussed.

Keywords: midwave, infrared, imaging, weather satellite, stereo, cloud motion vectors

1. INTRODUCTION

The science goals in the 2017 Earth Science Decadal Survey (DS17)[1] describe the needs for observations in the planetary boundary layers (PBL) and free troposphere of 3D winds to provide critical insights of cloud dynamics, convection and the large-scale circulation. Atmospheric dynamics are essential to the understanding of cloud-climate and cloud-precipitation processes, for which the community recommended: "Global measurements of the spatiotemporal (four-dimensional) evolution of large-scale horizontal wind vectors are urgently needed. It is important to avoid all or nothing strategies for the three-dimensional (3D) wind vector"[2, 3]. The decadal survey specifically calls for higher resolution observations of winds and cloud characteristics to improve scientific understanding and enable better forecasting of severe weather associated with tropical cyclones and midlatitude weather systems.

These critical wind measurements can be made using spaceborne active and passive methods of remote sensing (DS17). Achieving these measurements at the high spatial and temporal resolution required to meet science objectives in DS17 is a daunting challenge. The complementary strengths and weaknesses of active and passive systems suggests that a robust 3D wind measuring system will require both types. DS17 calls for incubation programs to explore the best combinations of active and passive sensors for a global wind architecture. While active methods such as lidar provide true three-dimensional winds with good vertical resolution and coverage in clear air, their narrow swath widths combined with their large size, weight, and power (SWaP) makes a constellation comprised solely of LIDARS economically infeasible for a space-based wind observing architecture. Passive winds can complement active methods by improving temporal and spatial coverage over a wide field of view (FOV).

Remote Sensing of the Atmosphere, Clouds, and Precipitation VII, edited by Eastwood Im, Song Yang, Proc. of SPIE Vol. 10776, 107760D · © 2018 SPIE
CCC code: 0277-786X/18/$18 · doi: 10.1117/12.2324612

A critical method for retrieving winds passively is atmospheric motion vectors (AMVs). Derived by tracking cloud or water vapor features in satellite imagery, AMVs are a proxy for direct measurements of the wind. AMVs are an important data source for initialization of numerical weather prediction (NWP) forecast models such as the Global Forecast System (GFS). Cloud motion vectors (CMVs) are a subset of AMVs in that the motion vectors are derived from cloud motions. However, a key issue for AMVs derived from satellite missions such as Geostationary Operational Environmental Satellite (GOES), Terra/Aqua, or the Joint Polar Satellite System (JPSS) is height assignment. Height assignment for these missions typically relies on the radiometric method.

The radiometric method depends on infrared emission at cloud top to derive a brightness temperature, which is then related to the local atmospheric temperature lapse rate. Elaborate multi-spectral methods have been developed such as the CO_2 slicing method[4,5] and H_2O intercept.[6] However, these methods require *a priori* knowledge of the atmospheric thermal structure and become problematic in the regions where atmospheric lapse rates are small or reversed.[7,8,9] It has been shown that height assignment based on standard radiometric methods (e.g. GOES and JPSS) exhibit mean differences compared to lidar of 2 km with a standard deviation of 3.4 km.[10]

MISR on NASA's *Terra* satellite has demonstrated that stereoscopic visible imaging can produce cloud motion vectors (CMVs) at good horizontal (17.6 km) and vertical (500 m) resolutions.[11,12] In contrast to GOES and JPSS, MISR relies on the parallax effect (Figure 1) for height assignment. Stereo methods depend on having at least two angular views of atmospheric objects (e.g. cloud, volcanic plume, aerosols) as the spacecraft moves in its orbit. The fore and nadir images intersect the cloud at times t_1 and t_2, respectively. The two-dimensional retrieval for cloud height is then given by[13]:

$$h_c = h_s - \frac{1}{tan(\theta_1)+tan(\theta_2)} d \equiv h_s - \alpha d. \quad (1)$$

The cloud geometric height (CGH) is determined by the angle to the surface normal at times t_1 and t_2 and the distance $d = v_S(t_2 - t_1)$ that the satellite travelled between the fore and nadir images that intersect the cloud. The error in cloud height is driven primarily by the ground sample distance (GSD) and the registration (for slowly moving objects). This simple technique provides an accurate estimate of cloud height regardless of time of day, surface brightness temperature, or atmospheric lapse rate. Key assumptions for stereo imaging are that the cloud persists in shape and location, and that it can be tracked and accurately geolocated in both images. The accuracy and precision of stereo-based wind retrievals can depend on the method used for pattern matching. In practice, the technique is usually applied to cloud patterns rather than to single elements.

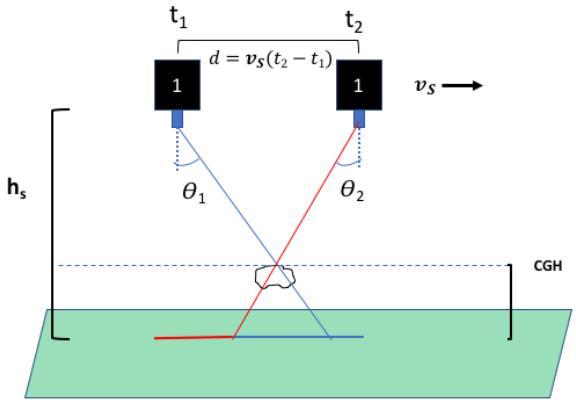

Figure 1: A schematic of the parallax effect used to estimate height for a single stationary object.

For cross-track cloud motions, CMVs and CGHs can be unambiguously calculated from a single satellite. However, if the cloud motions contain an along-track component, then an ambiguity is introduced for single-satellite retrievals, which results in correlated errors between CGHs and CMVs.[14] In fact, the height error for MISR CMVs is proportional to the error of the retrieved along-track motion.

A multiple-satellite approach can resolve the ambiguity by providing independent angular diversity.[15] For example, height assignment in LEO-GEO overlapped regions (Figure 2) can provide a practical approach to acquire multi-satellite retrievals. Figure 2 compares the MISR+GOES and MISR-only u and v winds, plus height assignment. We note that significant deviation from one-to-one correlation for both the v winds (i.e. predominately along track) and height assignment.

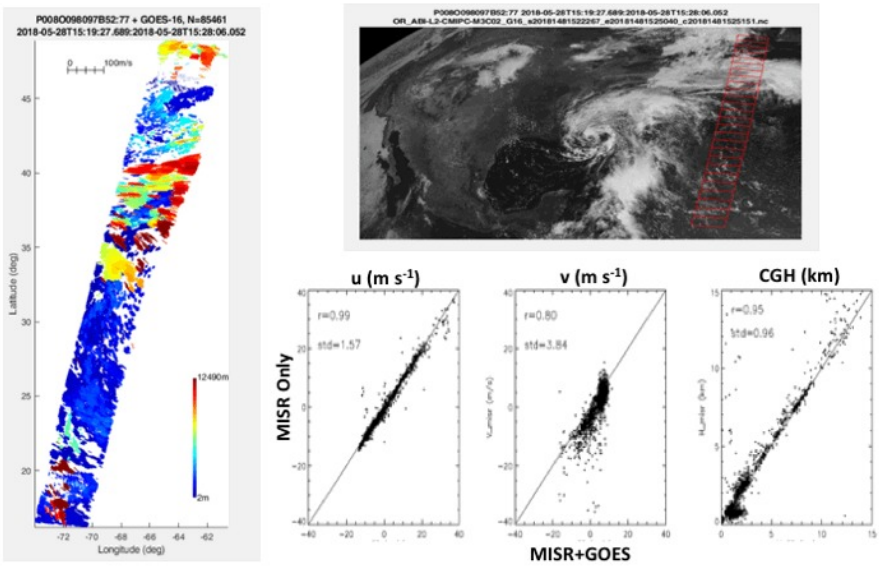

Figure 2: Multiple satellite approach for overlapped regions between MISR (left) and GOES-16 (top). The bottom images compare the u wind, v wind, and height assignment for GOES+MISR vs MISR-only.

Overlapped regions between LEO and GEO satellites can provide significantly improved accuracies for CMVs and CGHs as described above. However, LEO-GEO overlap has gaps in coverage over some ocean regions and both poles. A method for filling coverage gaps is to use two satellites in polar LEO orbits about 5-15 minutes apart. As shown in Fig. 3, the second satellite in such a LEO-LEO configuration would detect the cloud in the nadir view of its pushbroom imager at time $\tau + \Delta t$ after the nadir view from the first satellite, where τ is the time between the orbits of satellites 1 and 2, and Δt is the time increment due to the along-track motion of the cloud. The distance travelled by the cloud is Δd with along-track velocity given by $v_{\parallel} = \Delta d/(\tau + \Delta t)$.

The foregoing discussion suggests that a constellation of imagers in LEO would be ideal for stereo sensing of CGHs and CMVs. These instruments could be flown as stand-alone payloads on small satellites or has hosted payloads on a larger platform with a different primary mission.

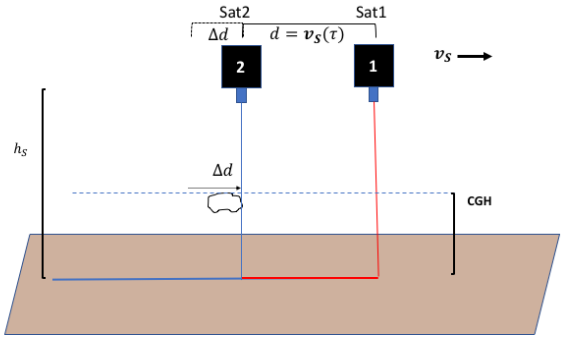

Figure 3: A schematic depicting the view of a cloud from two satellites in loose formation in order to resolve the ambiguity between CGH and CMV for along-track motion.

2. CONCEPT

The motivation for development of the Compact Midwave Imaging System (CMIS) is to advance the technical readiness level of a low-cost, low-SWaP imager that can fly initially as a two-satellite constellation in low-earth orbit (LEO). The purpose of such a mission would be to provide a passive component of a spaceborne wind monitoring system. A primary objective would be to compare/contrast the error characteristics between CGHs and CMVs obtained from LEO-GEO and LEO-LEO retrievals and to validate model calculations of spacecraft spacing needed to optimize the precision and accuracy of the retrievals. If a lidar was also flown (on one of the satellites), it would provide an opportunity to demonstrate the complementary nature of both modalities for retrieving 3D winds. The basic concept for the constellation is shown in Fig. 4.

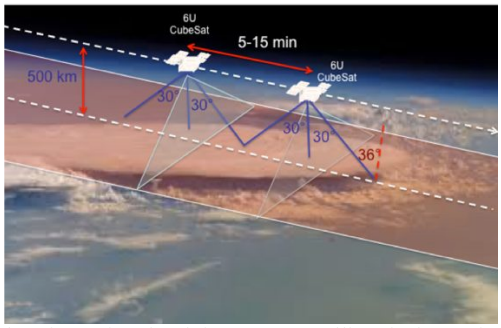

Figure 4: A schematic depicting the view of a cloud from two satellites in loose formation in order to resolve the ambiguity between CGH and CMV for along-track motion.

A key focus during the CMIS design effort was to keep the system very robust and very simple, while approaching the sensitivity and radiometric performance of exquisite instruments such as ABI, (Advanced Baseline Imager), MODIS (Moderate Resolution Imaging Spectroradiometer) and VIIRS (Visible Infrared Imaging Radiometer Suite). The system avoids the use of scanning mechanisms and requires only modest cooling to enable development of a low-SWaP, low-cost instrument that permits CMIS to be economically flown on a satellite constellation in LEO, thus permitting maximum temporal coverage and enabling study of secular phenomenologies revealed by the interactions of cloud top temperature (CTT), CMV and CGH.

The instrument design was optimized to retrieve accurate winds and cloud heights in the planetary boundary layer (PBL) and free troposphere as described in DS17. The shortwave/midwave infrared imager must be capable of 24/7 sensing at ground sample distance (GSD) < 1 km over a 50° field of view to provide wide-area coverage. The primary band for CGHs and CMVS will be 3.75 µm with the 4.05-µm band added to assist with CTT estimation. The Noise Equivalent δT (NEdT) must be < 1 K for background targets (i.e. clouds and volcanic ash) between 230 K and 300K to provide discrimination between multiple cloud layers. With ~5 stages of time-delay integration (TDI), it is anticipated that the FPA can sense clouds with CTT < 200 K, which suggests that cold cirrus should also be trackable. The longer wavelength channel is also useful for fire detection and volcanic ash dispersion. The 2.25-µm channel can be used to estimate and remove the solar component of the 3.75-µm channel during daytime operations. The SWIR channel also has utility for multi-spectral algorithms to estimate cloud optical depth and equivalent radius.

The utility of a 3.75-µm band can be understood as follows. VIIRS and MODIS have channels at 3.75 and 12 µm that allow for retrieval of CMVs at high precision. Both channels can sense cloud features at GSDs of 1 km or better during day and night. For this case, the 3.75-µm images exhibit more cloud texture or structures for extratropical cyclones compared to 12 µm. Fig. 5 shows that the correlation curve of image matching between VIIRS and MODIS has a narrower peak at 3.75 µm than at 12 µm, indicating that better precision for motion tracking can be achieved with 3.75 µm images due to the 3× better than 12-µm imaging for a given aperture. An airborne test campaign scheduled in 2019 with 3.75-µm and 12-µm imagers will be used to demonstrate that CMIS has the required sensitivity to resolve fine cloud structures (e.g. extratropical cyclones) needed to retrieve accurate CMVs and CGHs. The objective of the airborne campaign will be to show the potential of the low-SWaP, low-cost CMIS imager to meet requirements in DS17 for space-based wind and cloud-height retrievals.

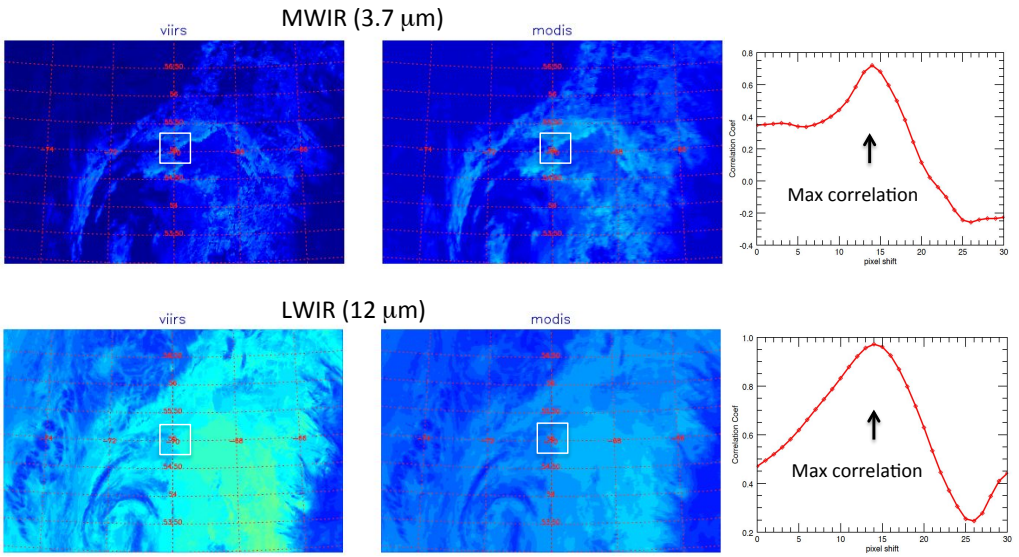

Figure 5: A cloud scene, taken by VIIRS and MODIS near (55°N, 70°W) on April 8, 2016 around UTC 1815 and gridded at 1-km resolution, shows a developing extratropical cyclone that can be readily seen in the 3.7 and 12 μm images. The white box indicates the region for pattern matching between VIIRS and MODIS, and the pattern matching correlation is showed in the red curve on the right panel. Both 3.7 and 12 μm images produce a shift of 14 pixels between VIIRS and MODIS, which corresponds to ~45 m/s cloud motion as the images were taken ~5 min apart.

3. INSTRUMENT

The CMIS instrument consists of three bands at 2.25 μm, 3.75 μm, and 4.05 μm for sensing clouds, aerosols, and atmospheric particulates. CMIS employs pushbroom imaging with a butcher block stripe filter installed immediately above the focal plane array (FPA). The butcher block filter design is shown in Fig. 6. Notice the three stripes at the top, middle, and bottom at 3.75 μm to provide aft, nadir, and fore views, respectively for stereo sensing.

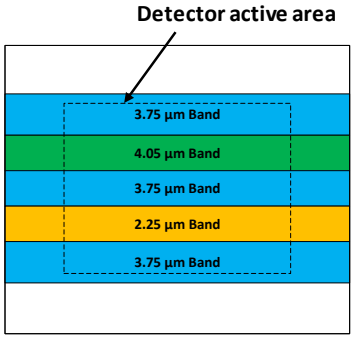

Figure 6. Stripe filter concept with fore, nadir and aft views at 3.75 um for stereo imaging along with stripes for imaging at 2.25 μm (orange) and 4.05 μm. The dashed-line rectangle shows the active area of the 640×512 FPA.

The system utilizes a single optic, a single detector, and a single stripe filter. It employs telecentric optics to minimize incident angles, thereby enabling narrow-band imaging. Cooled optics minimize the background signal from thermal self-emission. The original concept was to use a thermoelectric cooler to cool the optics, but our analysis revealed that a small Stirling cooler provides more cooling at lower power. Table 1 shows the center wavelengths and bandwidths of each channel. Band 2 (3.75 μm) will be the primary channel used for stereo calculations.

Table 1: CMIS Channel Characteristics

Band	Center Wavelength (μm)	Bandwidth (nm)	SNR/NEdT
1	2.25	50	100
2	3.75	180	<1K between 230-270 K
3	4.05	100	<1K between 230-270 K

Fig. 7 shows the mechanical design of CMIS. The SWaP is estimated to be 105 mm × 96 mm × 185 mm, 2 kg, and 8 W, which should fit comfortably in a 6-U CubeSat form factor. After a detailed selection process for the detector, the CMIS team chose a Type-2 Super Lattice (T2SL) detector hybridized onto a 640 × 512 readout integrated circuit with a 15-μm pixel pitch. Calibration device and baffle are not shown.

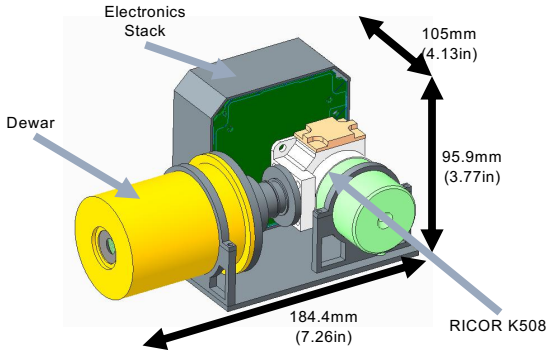

Figure 7: Mechanical layout of the CMIS instrument.

T2SL detector technology was chosen because it provides excellent sensitivity for 24/7 sensing across a wide temperature range and high operating temperature ($T_{detector}$=150 K), which makes it feasible for small satellites due to its reduced power draw. Recent measurements at APL demonstrated that dark current levels for a T2SL detector with a 5-μm cutoff wavelength are a factor of 2.3 above the "Rule 07" level predicted for the best HgCdTe detectors and 2 times *lower* than that predicted for HgCdTe in the LWIR (12-μm cutoff wavelength). Thus, it was expected that the dark current for an MWIR T2SL detector with 4.2-μm cutoff wavelength would be low at an operating temperature of 150 K so as to provide the radiometric performance necessary for CMIS.

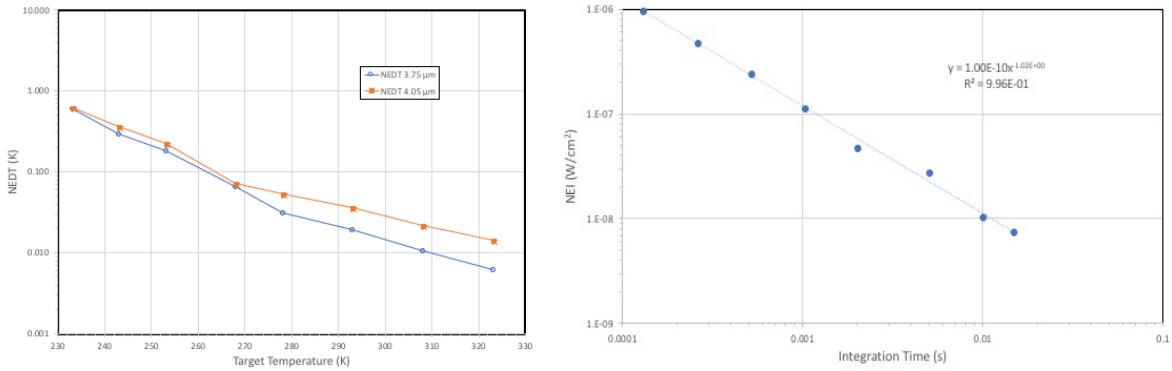

Figure 8: NEdT (left) and NEI (right) for CMIS channels 3.75 and 4.05 μm, and 2.25 μm (right).

Recent measurements of the flight T2SL detectors for CMIS bear this out. Fig. 8 shows that the NEdT for both the bands 2 and 3 (left) are less than 1K at 230 K with the 200-nm bandwidth filters. The bandwidth for the flight filters will be 180 nm, which implies that the NEdT should be ~1 K at 230 K for both bands. Furthermore, our calculations indicate that five stages of time-delay integration (TDI) should result in an NEdT = ~2 K for Bands 2 and 3 at 200 K. The noise equivalent irradiance (NEI) for band 1 (2.25 μm) decreases linearly with irradiance. At 15 ms, the NEI is approximately

7.6×10^{-9} W cm^{-2}, which gives an SNR = ~100 for reflected sunlight, assuming the albedo $\alpha = 0.25$. This demonstrates that CMIS has excellent sensitivity and can detect and characterize clouds throughout the entire depth of the troposphere.

Fig. 9 shows the filter transmission and quantum efficiency for detector temperature at 150 K of each band as a function of wavelength. The cutoff wavelength for the FPA was specified to be at 4.2 µm, but the actual cutoff for this particular set of FPAs is somewhat short of the specification. The QEs for bands 1 and 2 are better than that for band 3. However, all three channels meet requirements for a space mission to retrieve CMVs and CGHs.

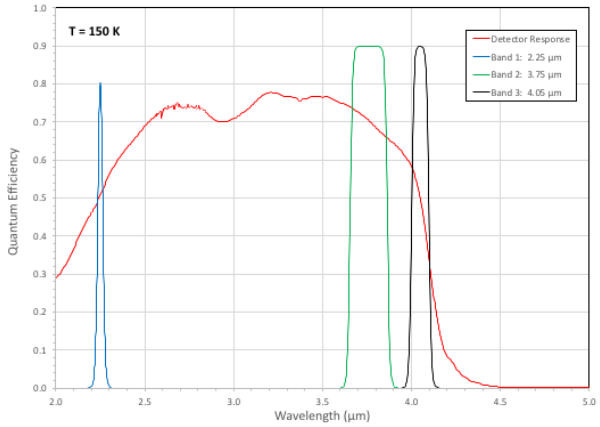

Figure 9: Quantum efficiency for CMIS focal plane array overlaid by filter transmissions for Bands 1, 2, and 3.

4. MODEL

The CMIS concept is based primarily on the stereo method applied to multiple satellites to achieve the precision and accuracy requirements for wind specified in DS17. A key aspect of exploiting these wind measurements will be the assimilation of CMVs into numerical weather prediction (NWP) models. However, modern data assimilation systems require error covariance statistics for proper weighting of the observations.[16]

Our initial simplified calculations estimated the mean errors that result from tracking a low-cloud layer with uniform heights in a horizontally and vertically uniform wind field. Individual cloud elements were specified with a uniform wind profile to estimate accuracy. Using the wind speed to correct the cloud height with image registration accurate to ½ pixel for 700-m GSD and 50° FOV, the mean error of the CGH was 295 m. A real-world analogue for such an idealized case might be a field of relatively uniform stratocumulus clouds.

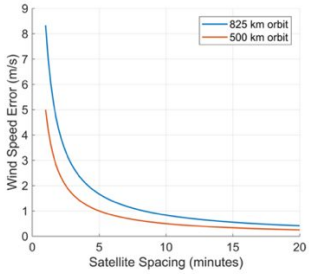

Figure 10: Estimated wind speed error as a function of satellite spacing for a simple first order model.

Fig. 10 shows the dependence on satellite spacing of the mean error for the CMVs. As the time between satellite passes increases, the clouds move farther in this uniform wind case, and so errors in geolocation are minimized. This simple model can be fairly representative for stable regimes where the lifetimes of individual clouds are long, but cannot be considered representative for regimes with rapid cloud evolution.

To provide realism over a broader set of cases, it became apparent that a more sophisticated, realistic end-to-end modeling capability is needed. The model must reliably and scalably simulate CMIS data from either single or multiple imagers, for both airborne and space platforms, incorporate a pushbroom configuration mode, and tie in the FPA performance measurements. As we develop the sensor model, we envision designing and testing the entire CMIS algorithm pipeline in parallel with hardware development in a way that allows real data to be substituted as directly as possible once the sensor comes online. An important use for our end-to-end model is to gather and compare stereo retrieval statistics over a broad range of different cases. This ability to compare stereo retrievals with simulated data has allowed us to start developing, testing, and inter-comparing cloud matching algorithms in an objective way.

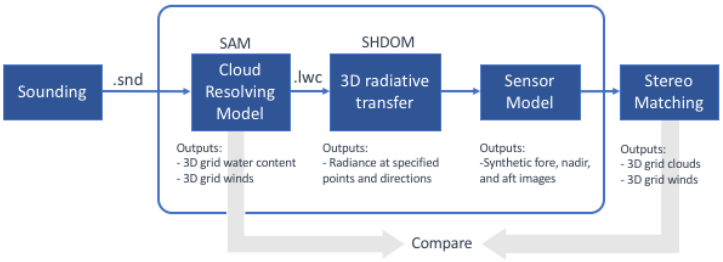

Figure 11: End-to-end components for CMV performance estimate.

A prototype of the end-to-end CMIS Simulator as shown in Fig. 11 has been developed. It is designed to provide realistic cloud scenes to evaluate the performance of CMIS retrievals for CMVs and CGHs for various dynamical regimes. The first step in the process is to run the System for Atmospheric Modeling[17] (SAM) for specific cases of interest. We chose SAM because it uses first-principles physics to simulate specific cases with desired cloud characteristics, such as multiple moist layers in a sounding to produce multiple cloud layers, and gives access to a wide range of parameters that can be initialized, forced, and observed. After the cloud fields are generated, the next step is to run the Spherical Harmonics Discrete Ordinate Model[18,19] (SHDOM) to calculate radiances in the fore, nadir, and aft viewing geometries of CMIS. These radiances are then fed into the sensor model, which simulates the optical performance of CMIS, and includes realistic effects such as spacecraft jitter. After the radiometric calibration is applied, the model performs geolocation and applies pattern matching to identify clouds that can be tracked. The CMVs and CGHs are then calculated using a baseline optical flow pattern matching algorithm and validated against the wind field obtained from SAM.

Pixel matching between two successive image frames can be accomplished by a form of block matching or by optical flow. Block matching works by extracting a block in the neighborhood of a reference pixel, and optimizing a matching criterion (e.g., mean squared error, or mean absolute difference) in a translated version of the block in the target image. Optical flow based methods assume that each pixel in a reference image shifts by some amount to the target image, and combine the idea of brightness constancy, i.e., that a pixel does not change in intensity as it is translated from the reference to the target, with a model for the neighborhood of a pixel. Both approaches can be tuned to perform well in a variety of retrieval settings. However, both approaches can suffer from a variety of matching errors resulting in incorrect retrievals if mistuned. In practice, we found optical flow methods more robust, faster, and easier to tune, and used a simple Farnebäck algorithm[20] in our baseline wind retrievals. As evidenced by recent advances in the performance of stereo and optical flow retrieval algorithms on benchmarks such as Middlebury Stereo[21] and KITTI[22], a more sophisticated matching algorithm will help increase wind retrieval performance.

JHU/APL leveraged the CMIS simulator to model the formation and movement of a marine stratocumulus layer off the coast of California using dropsonde data from the Second Dynamics and Chemistry of Marine Stratocumulus field study (DYCOMS-II), flight RF02, conducted on 11 July 2001. We were able to simulate views of a single cloud layer as it would appear to an orbital imager in the three CMIS bands, as well as in the visible band (for testing). A large scale constant wind forcing was presented to the simulator, and the cloud scene was evolved in 10s increments to produce synthetic CMIS imagery over time. The retrieval results for this relatively simple case are shown above. Figure 12 shows the evolved wind field overlaid on a visible rendering of the cloud layer as viewed from orbit, and the retrieved horizontal wind components as determined by optical flow from two images 15 minutes apart. For this simple case with marine stratocumulus and uniform wind speeds, the time difference of the orbits does not have a significant impact on

wind retrieval accuracy. Over 90% of the 12,087 retrieved wind components were within ±1.0 m/s of their expected value.

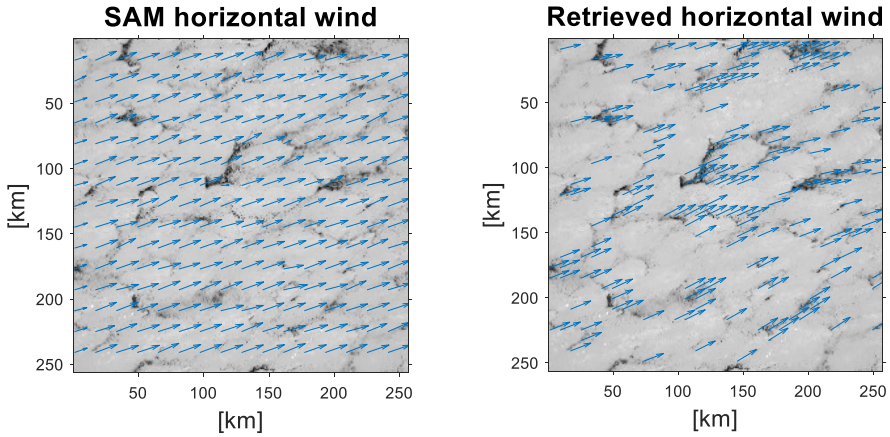

Figure 12: Simulated (SAM) and retrieved horizontal CMV components over a representative 256-by-256 km domain, overlaid on top of a visible rendering of the cloud layer as viewed from orbit. A retrieval was only made in areas of high cloud texture.

5. SUMMARY AND CONCLUSIONS

This paper describes a new instrument, CMIS, that has been designed to retrieve CMVs and CGHs to meet key science objectives in DS17. The instrument employs T2SL detector technology, which allows for operation at much warmer temperatures than conventional detectors. The low-cost and low-SWaP CMIS instrument will make it possible to deploy a constellation of these instruments in LEO to provide high refresh rates for cloud heights, temperatures and wind patterns. The program will begin fabrication over the next three months followed by testing and flight qualification prior to an airborne demonstration scheduled for the Fall of 2019.

A simulator is under development to generate performance statistics for CMIS over a wide range of different cloud types and climate regimes. This simulator will be developed to accept either simulated data from an atmospheric model (e.g. SAM) or from instruments flown on aircraft or space platforms. The current pattern matching algorithm used for the CMIS simulator is a simple optical flow method. The objective will be to collaborate with the stereo community to evaluate different pattern matching schemes and retrieval methodologies for CMIS.

ACKNOWLEDGEMENTS

The authors are grateful for funding provided under NASA Earth Science Technology Office IIP Grant NNX17AG65G.

REFERENCES

[1] The National Academies of Sciences, Engineering, Medicine, "Thriving on our Changing Planet: A Decadal Strategy for Earth Observation from Space" (2017).
[2] NASA (2014), https://espo.nasa.gov/home/content/NASA_SMD_Workshop
[3] NASA (2015), http://science.nasa.gov/media/medialibrary/2015/08/03/Weather_Focus_Area_Workshop_Report_2015.pdf
[4] Baum, B. A., and B. A. Wielicki, "Cirrus cloud retrieval using infrared sounder data: Multilevel cloud errors", J. Appl. Met., 33, 107-117 (1994).
[5] Frey, R. A., B. A. Baum, W. P. Menzel, S. A. Ackerman, C. C. Moeller, and J. D. Spinhirne, "A comparison of cloud top heights computed from airborne lidar and MAS radiance data using CO_2 slicing" , *J. Geophys. Res.*, *104*, 24,547–24,556 (1999)
[6] Schemtz, J., K. Holmlund, J. Hoffman, B. Strauss, "Operational Cloud-Motion Winds from Meteosat Infrared Images", *J. App. Met*. 32, 1206-1225 (1993)

[7] Manizade, K.F., J. D. Spinhirne, R. S. Lancaster, "Stereo cloud heights from multispectral IR imagery via Region-of-Interest Segmentation", IEEE Trans. Geo and Rem Sens., 44(9), 2481-2491 (2006).
[8] Holz, R.E., S.A. Ackerman, F.W. Nagle, R. Frey, S. Dutcher, R.E. Kuehn, M.A. Vaughan, and B. Baum, "Global Moderate Resolution Imaging Spectroradiometer (MODIS) cloud detection and height evaluation using CALIOP", J. Geophys. Res., 113, (2008) D00A19,doi:10.1029/2008JD009837.
[9] Garay, M.J., S.P. de Szoeke, and C.M. Moroney (2008), Comparison of marine stratocumulus cloud top heights in the southeastern Pacific retrieved from satellites with coincident shipbased observations, J. Geophys. Res., 113, D18204 (2008) doi:10.1029/2008JD009975.
[10] DiMichele, S., T.McNally, P. Bauer, and I. Genkova, 2013: Quality assessment of cloud-top height estimates from satellite IR radiances using the CALIPSO lidar. IEEE Trans.Geosci. Remote Sens., 51, 2454–2464, (2013) doi:10.1109/TGRS.2012.221072
[11] Horváth, A. and R. Davies, "Feasibility and Error Analysis of Cloud Motion Wind Extraction from Near-Simultaneous Multiangle MISR Measurements", *J. Atmos. Oc. Tech*, **18**, 591-608 (2001).
[12] Muller, J.-P., A. Mandanayake, C. Maroney, R. Davies, D.J. Diner, and S. Paradise, "MISR Stereoscopic Technique Image Matchers : Techniques and Results", *IEEE Trans. Geo. Rem. Sens*. **40,** 1547-1559 (2002)
[13] Zong, J., R. Davies, J.-P., Muller, and D.J. Diner, "Photogrammetric retrieval of cloud advection and top height from the Multi-angle Imaging Spectroradiometer (MISR)", Photogramm. Eng. Remote Sens., 68, 821–829 (2002)
[14] Mueller, K. J., D. L. Wu, A. Horvath, V. M. Jovanovic, J.-P. Muller, L. Di Girolamo, M. J. Garay, D. J. Diner, C. M. Moroney, S. Wanzong, "Assessment of MISR Cloud Motion Vectors (CMVs) Relative to Goes and MODIS Atmospheric Motion Vectors (AMVs)", *J. Appl. Met. Clim*., **56,** 555-572 (2017)
[15] Carr, J., "Multi-Satellite 3D Winds", NOAA Emerging Technologies Workshop, August 2017 (2017).
[16] Fairbairn D, Pring SR, Lorenc AC, Roulstone I., "A comparison of 4DVar with ensemble data assimilation methods", *Q. J. R. Meteorol. Soc.* **140**: 281–294 (2014). DOI:10.1002/qj.2135
[17] Khairoutdinov, M. F. and D. A. Randall, "Cloud-resolving modeling of the ARM summer 1997 IOP: Model formulation, results, uncertainties and sensitivities", J. Atmos. Sci., 60, 607-625 (2003).
[18] Evans, K. F., "The spherical harmonic discrete ordinate method for three-dimensional atmospheric radiative transfer", *J. Atmos. Sci.,* **55,** 429-446 (1998)
[19] Pincus, R., and K. F. Evans, "Computational cost and accuracy in calculating three-dimensional radiative transfer: Results for new implementations of Monte Carlo and SHDOM", *J. Atmos. Sci.,* **66,** 3131-3146 (2009)
[20] Farnebäck, G., Two-frame motion estimation based on polynomial expansion. In Proceedings of the 13th Scandinavian Conference on Image Analysis, 363-370 (2003)
[21] Scharstein, D., and R. Szeliski. A taxonomy and evaluation of dense two-frame stereo correspondence algorithms. *International Journal of Computer Vision*, 47(1/2/3):7-42, (2002)
[22] Menze, M., C. Heipke, A. Geiger, "Object Scene Flow", *ISPRS Journal of Photogrammetry and Remote Sensing (JPRS)*, (2018)